

Spline-Based Rotor and Stator Optimization of a Permanent Magnet Synchronous Motor

1st Michael Wiesheu

Computational Electromagnetics Group
Technical University of Darmstadt
 Darmstadt, Germany
 michael.wiesheu@tu-darmstadt.de

2nd Theodor Komann

Department of Mathematics
Technical University of Darmstadt
 Darmstadt, Germany
 komann@mathematik.tu-darmstadt.de

3rd Melina Merkel

Computational Electromagnetics Group
Technical University of Darmstadt
 Darmstadt, Germany
 melina.merkel@tu-darmstadt.de

4th Sebastian Schöps

Computational Electromagnetics Group
Technical University of Darmstadt
 Darmstadt, Germany
 sebastian.schoeps@tu-darmstadt.de

5th Stefan Ulbrich

Department of Mathematics
Technical University of Darmstadt
 Darmstadt, Germany
 ulbrich@mathematik.tu-darmstadt.de

6th Idoia Cortes Garcia

Department of Mechanical Engineering
Eindhoven University of Technology
 Eindhoven, The Netherlands
 i.cortes.garcia@tue.nl

Abstract—This work features the optimization of a Permanent Magnet Synchronous Motor using 2D nonlinear simulations in an Isogeometric Analysis framework. The rotor and stator designs are optimized for both geometric parameters and surface shapes via modifications of control points. The scaling laws for magnetism are employed to allow for axial and radial scaling, enabling a thorough optimization of all critical machine parameters for multiple operating points. The process is carried out in a gradient-based fashion with the objectives of lowering motor material cost, torque ripple and losses. It is shown that the optimization can be efficiently conducted for many optimization variables and all objective values can be reduced.

Index Terms—Isogeometric Analysis, Parameter Optimization, Permanent Magnet Synchronous Motor, Shape Optimization

I. INTRODUCTION

Optimizing electric machines is a challenging task. On the one hand, there are a variety of options to change the geometric design, e.g., parameters (such as magnet width, yoke thickness or motor length) or shape adjustments (such as the rotor and stator surfaces). This can lead to a high dimensional design space. On the other hand, there are multiple quantities of interest which should be improved, such as the motor cost, performance (given quantified e.g. by the motor torque), or efficiency.

This has led to a variety of published research articles and surveys that feature Finite Element (FE) based optimization of e.g. cost [1] or torque ripple [2] with methods such as parameter optimization [3], shape optimization [4] or topology optimization [5]. Gradient-free algorithms, like particle swarms or genetic algorithms, are commonly applied in these studies due to their simplicity and promise of achieving a global optimum. Yet, these approaches can become computationally expensive when the optimization has a large design space, i.e., there are many variables to optimize.

This work extends the previously proposed method in [6], where the rotor of a Permanent Magnet Synchronous Machine (PMSM) is optimized for both parameters and shape with

gradient based optimization. Here, both, the rotor and stator parameters and surfaces are optimized, and multiple operating points are considered for a different motor geometry. A snapshot of the code can be found in [7].

II. METHODOLOGY

This section briefly describes the underlying numerical methods and optimization techniques. It focuses on new features that are not covered in the previous work [6], which contains methodological explanations in detail. For more information, the interested reader is also referred to preliminary work deriving the mathematical foundations [8, 9].

A. Numerical modeling

To describe the electromagnetic behavior of the electric machine, we employ the magnetostatic problem

$$\nabla \times (\nu \nabla \times \mathbf{A}) = \mathbf{J} + \nabla \times (\nu \mathbf{B}_r), \quad (1)$$

with the magnetic vector potential \mathbf{A} , the (nonlinear) reluctivity ν , the current source density \mathbf{J} and the magnet remanence \mathbf{B}_r . The magnetic flux density \mathbf{B} is defined via $\mathbf{B} = \nabla \times \mathbf{A}$. This formulation is common for PMSM machines, where eddy currents are neglected due to the lamination of the iron cores [10]. Reducing (1) to 2D and considering rotor and stator domains Ω_{rt} and Ω_{st} separately yields the Poisson problem

$$\begin{cases} \nabla \cdot (\nu \nabla A_{z,rt}) = \nu \nabla \cdot \mathbf{B}_r^\perp & \text{in } \Omega_{rt} \\ \nabla \cdot (\nu \nabla A_{z,st}) = -J & \text{in } \Omega_{st}, \end{cases} \quad (2)$$

where $\mathbf{A} = (0 \ 0 \ A_z)^\top$. Homogeneous Dirichlet boundaries are applied at Γ_d , antiperiodic ones at Γ_{ap} and the coupling of rotor and stator is performed at the air gap interface Γ_{ag} , see Fig. 1. 3D effects, e.g. due to the end windings, will be neglected. The right-hand side in (2) is given by the 2D components of the remanence and the three phase current. The 2D remanence is given by $\mathbf{B}_r^\perp = B_r (-\sin(\alpha) \ \cos(\alpha))^\top$

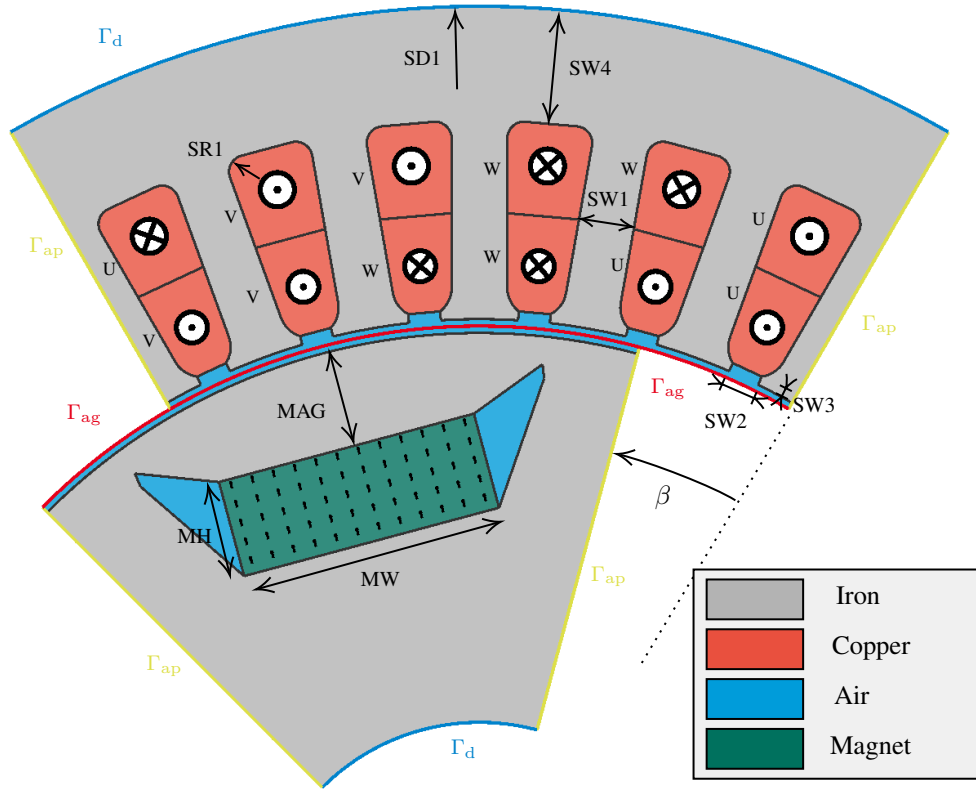


Fig. 1: Parametrization of the PMSM geometry including parameter names, material definitions and boundary conditions. The model is originally based on [11].

defined by the remanence B_r and orientation α and the three phase current is given by $J = \sum_k J^{(k)}$ with

$$J^{(k)} = J_0 \sin\left(p\beta + \varphi_0 + \frac{2\pi}{3}k\right), \quad (3)$$

where $k \in \{0, 1, 2\}$ indicates the k -th phase. For synchronous operation, this can be expressed by a current density J_0 , the pole pair number p , the electric phase offset φ_0 and the rotation angle β .

The PMSM considered in this work is illustrated in Fig. 1. Due to symmetry, only one sixth of the motor is simulated. The rotor and stator iron cores are shown in gray, the (homogenized) copper slots in red, the rotor magnet in green and the air gap and air pockets in blue. In addition, the parameter names for later optimization are given.

Discretization of (2) with Isogeometric Analysis (IGA) and coupling of the rotor and stator surface with Harmonic Mortaring [9] yields the matrix system

$$\underbrace{\begin{pmatrix} \mathbf{K}_{rt} & \mathbf{0} & -\mathbf{G}_{rt} \\ \mathbf{0} & \mathbf{K}_{st} & \mathbf{G}_{st}\mathbf{R}_\beta \\ -\mathbf{G}_{rt}^\top & \mathbf{R}_\beta^\top \mathbf{G}_{st}^\top & \mathbf{0} \end{pmatrix}}_{=: \mathbf{K}} \underbrace{\begin{pmatrix} \mathbf{u}_{rt} \\ \mathbf{u}_{st} \\ \lambda \end{pmatrix}}_{=: \mathbf{u}} = \underbrace{\begin{pmatrix} \mathbf{b}_{rt} \\ \mathbf{b}_{st} \\ \mathbf{0} \end{pmatrix}}_{=: \mathbf{b}} \quad (4)$$

with the stiffness matrices \mathbf{K}_{rt} and \mathbf{K}_{st} , coupling matrices \mathbf{G}_{rt} and \mathbf{G}_{st} , the rotation matrix \mathbf{R}_β depending on the rotation angle β , the magnetic potential \mathbf{u}_{rt} and \mathbf{u}_{st} , the Lagrange

multipliers λ and the right-hand side \mathbf{b}_{rt} and \mathbf{b}_{st} . Because of the Harmonic Mortaring, only the rotation matrix \mathbf{R}_β , which contains sine and cosine function values, needs to be recalculated for different β . For conciseness, (4) is rewritten as the state equation

$$\mathbf{e}(\mathbf{u}) = \mathbf{K}(\mathbf{u})\mathbf{u} - \mathbf{b}, \quad (5)$$

where \mathbf{K} depends also on \mathbf{u} due to material nonlinearities. After solving (5) with a Newton scheme, the electromagnetic torque T_β of the motor is determined with

$$T_\beta(\mathbf{u}) = -\mathbf{u}_{st}^\top \mathbf{G}_{st} \mathbf{R}'_\beta \lambda L k_R^2 \quad (6)$$

by introducing the motor length L and the radial scaling k_R .

Evaluating (6) for multiple $\beta \in \{\beta_1, \beta_2, \dots, \beta_N\}$, we can calculate the average torque \bar{T} and the torque standard deviation \hat{T} with

$$\bar{T} = \frac{1}{N} \sum_\beta T_\beta \quad \hat{T} = \sqrt{\frac{1}{N} \sum_\beta (T_\beta - \bar{T})^2}. \quad (7)$$

The average torque is linked to the motor power and the torque standard deviation influences the rotation smoothness, so both values are relevant quantities to be optimized.

B. Scaling laws for the Finite Element solution

For convenience in the following optimization steps, scaling laws of the FE solution are introduced [12, 13]. This allows

for the inclusion of the motor's radial scaling (given by k_R) and axial length (given by L) as optimization variables. Table I summarizes the necessary variables and their respective scaling with respect to k_R and L .

TABLE I: Scaling laws with respect to k_R and L , according to [12].

Parameter	Variable	α
Magnetic flux density	\mathbf{B}	1
Magnetic field strength	\mathbf{H}	1
Cross sectional area	A	k_R^2
Stator current	I	k_R
Stator current density	J	k_R^{-1}
Torque	T	$k_R^2 L$
Material cost	M	$k_R^2 L$

Note that the stator current I must increase by k_R in order for the magnetic field to remain unchanged if radial scaling k_R is applied. That implies a scaling of the current density J by k_R^{-1} , which can lead to unrealistic results, as the maximum current density can not be increased arbitrarily. Therefore, we scale the current density from (3) by k_R , such that J_0 in the final configuration always remains the same.

For the optimization, we further calculate the motor material cost M by

$$M = L k_R^2 \sum_i \rho_i A_i c_i \quad (8)$$

with the material density ρ_i , cross sectional A_i and cost per mass c_i for the i -th material, respectively. In addition to M we define the Joule stator losses P_J [14] for one slot as

$$P_J = C A_{\text{slot}} L, \quad (9)$$

where C is a constant taking into account the stator current density, conductivity and number of windings. This is the only loss mechanism considered here and is used to penalize less efficient designs.

For the necessary derivatives in the gradient based optimization, the simple relationships

$$\begin{aligned} \frac{dT}{dL} &= \frac{T}{L} & \frac{dT}{dk_R} &= 2 \frac{T}{k_R} \\ \frac{dM}{dL} &= \frac{M}{L} & \frac{dM}{dk_R} &= 2 \frac{M}{k_R} \\ \frac{dP_J}{dL} &= \frac{P_J}{L} & \frac{dP_J}{dk_R} &= 2 \frac{P_J}{k_R} \end{aligned} \quad (10)$$

can be exploited in addition to the derivatives given in [6] to include the radial and axial dimensions.

C. Optimization

The objective function consists of three components that should be minimized: the motor mass M , the torque ripple \hat{T} and the Joule losses P_J . We employ a multi-objective optimization approach with a weighted sum, i.e., every objective is scaled by a weight m_i . The torque ripple is evaluated for different operating points and summed up in \hat{T} . Here, we choose the operating points in the set $J \in J_0 \cdot \{0, 0.5, 1\}$ and

$\beta \in \{0, 2, \dots, 18\}$ reducing both cogging torque and the torque ripple.

As constraints, first, the magnetostatic formulation (5) must be fulfilled. Second, the mean torque \bar{T} must meet the target value T_{Target} . Third, geometric constraints \mathbf{g} are applied, such that there are no overlaps between different domains. Overall, the optimization problem is written as

$$\begin{aligned} \min f_{\text{opt}}(\mathbf{x}, \mathbf{u}) &= m_1 M + m_2 \hat{T} + m_3 P_J \\ \text{s.t.} & \\ \left\{ \begin{array}{ll} \mathbf{e}(\mathbf{x}, \mathbf{u}) = \mathbf{0} & \text{State equation} \\ \bar{T} \geq T_{\text{Target}} & \text{Fulfill target torque} \\ \mathbf{g}(\mathbf{x}) \leq \mathbf{0} & \text{Geometric feasibility.} \end{array} \right. & (11) \end{aligned}$$

The design vector \mathbf{x} contains the parameters shown in Fig. 1, the variables φ_0 , L , k_R as well as the radial offsets of the rotor and stator surface control points.

The derivatives of (11) are calculated with (10) as well as the analytical derivatives from [6] using the adjoint method. This allows for an efficient optimization process despite the large number of design variables.

III. RESULTS

The optimization is carried out with *MATLAB*[®]'s solver *fmincon* using the *interior-point* method in an IGA framework with *GeoPDEs* [15]. The material cost is chosen as a dimensionless number with $c_{\text{Iron}} = 2$, $c_{\text{Copper}} = 10$ and $c_{\text{Magnet}} = 50$ to roughly represent the proportion of real material cost. The objective weights in Eq. (11) are set to $m_1 = 0.05$ $m_2 = 10$ $m_3 = 4$ such that the different objectives are of comparable magnitude. The maximum current density is set to $J_0 = 3.2 \text{ A mm}^{-2}$. As torque requirement, a torque of $T_{\text{Target}} \geq 1.5 \text{ Nm}$ must be maintained. For the iron, the nonlinear BH-characteristics of M330-50A (M27) is used [16]. Table II summarizes the initial parameter values with lower and upper bounds.

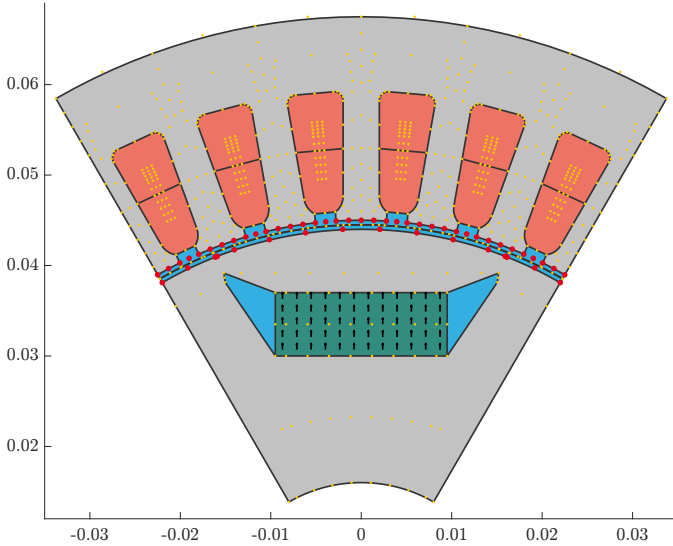
TABLE II: Motor parameters and bounds for the optimization.

Parameter name	initial	min	max	opt
L	100 mm	80 mm	120 mm	80 mm
φ_0	0 deg	-20 deg	20 deg	-11.6 deg
k_R	1	0.5	2	1.048
MAG	7 mm	6 mm	15 mm	6.10 mm
MH	7 mm	2 mm	12 mm	2.74 mm
MW	19 mm	10 mm	25 mm	20.73 mm
SD1	135 mm	90 mm	160 mm	130.29 mm
SR1	1 mm	0.5 mm	2 mm	2.0 mm
SW1	4 mm	2 mm	6 mm	4.06 mm
SW2	2.3 mm	1 mm	4 mm	1.0 mm
SW3	1 mm	0.5 mm	1.5 mm	0.50 mm
SW4	8.25 mm	2 mm	20 mm	5.43 mm

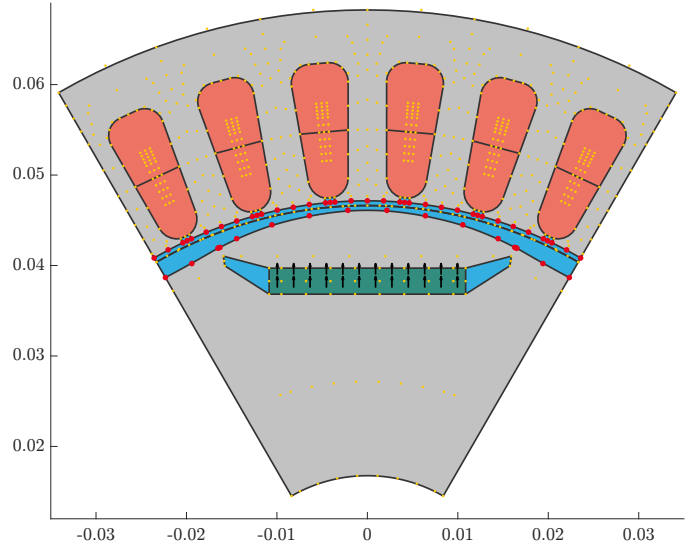
Overall, there are 22 design variables, where 12 come from the parameters and 10 from the (symmetrically chosen) control points. The FE simulation is carried out with 4095 degrees of freedom and 741 control points. These are highlighted in Fig. 2a, where the initial and geometry is shown. The magnetic flux density for the initial design at $\beta = 0^\circ$ is shown in Fig. 3a.

The optimization is carried out on a 8-core laptop¹ in 120

¹Intel[®] Core[™] i7-1165G7@2.8GHz with 16 GB RAM.

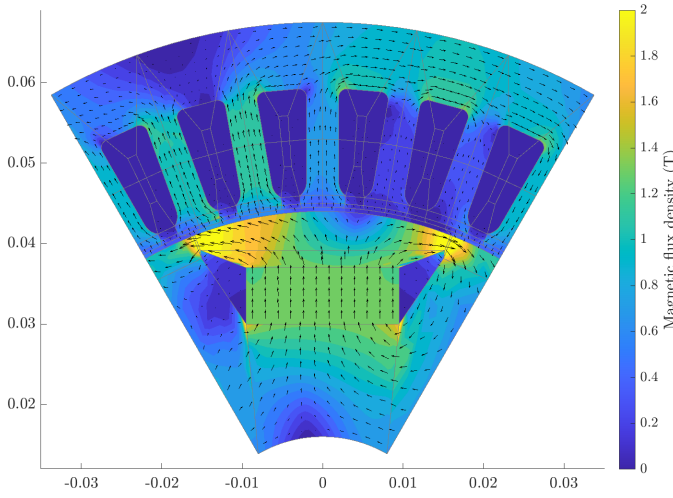


(a) Geometry representation of the initial motor geometry.

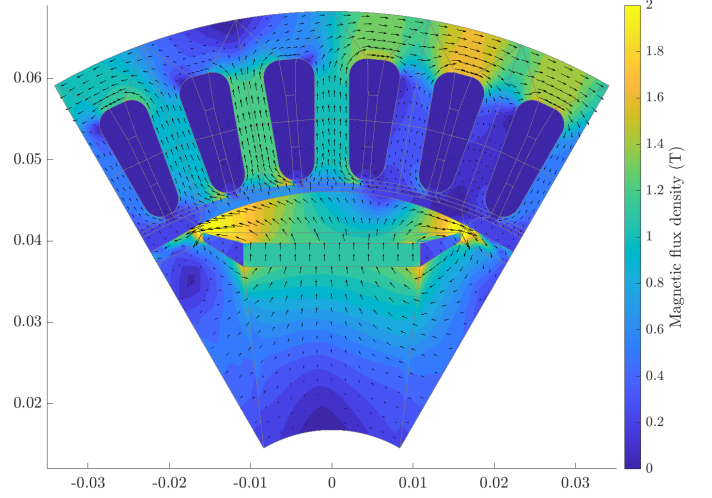


(b) Geometry representation of the optimized motor geometry.

Fig. 2: Comparison of initial and optimized geometry. The yellow points show the control points of the motor, the red control points may move during the optimization.



(a) Magnetic flux density of the original motor.



(b) Magnetic flux density of the optimized motor.

Fig. 3: Comparison of the magnetic flux density.

iterations within six hours. The results of the optimization are presented in Table III. The optimized geometry is given in Fig. 2b. Two features of the new geometry are that the magnet size is greatly reduced, leading to a lower cost and that the rotor surface is not circular any more, which reduces the torque ripple. As there is a trade off between magnet size (influences cost) and the coil size (influences loss), the weights in (11) can be further adjusted to generate multiple designs in a Pareto front. The distribution of the magnetic flux density for the optimized design is shown in Fig. 3b.

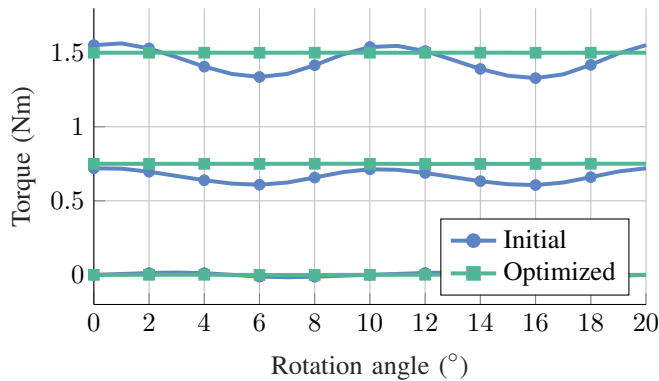
The findings can be summarized as follows:

- The motor cost, torque ripple and power loss can be reduced. The decrease is 35.0%, 99.0% and 4.42% respectively.

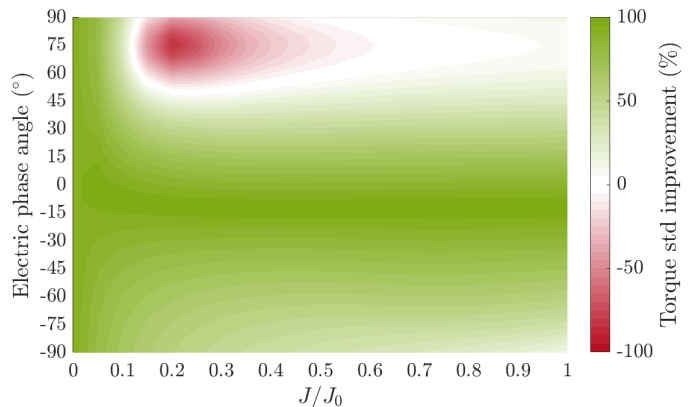
TABLE III: Comparison of objectives for the initial and optimized motor.

	Initial	Optimized	Change
f_{opt}	2.0555	0.5743	-72.1%
Cost Motor	11.1506	7.2520	-35.0%
Cost Iron	2.534	2.1006	-17.1%
Cost Copper	3.6291	3.2774	-9.69%
Cost Magnet	4.9875	1.8739	-62.4%
Torque Ripple at OP	0.129	0.0013	-99.9%
Power Loss	0.0520	0.0497	-4.42%

- Compared to the initial design (Fig. 3a), the magnetic flux density in the optimized design (Fig. 3b) is increased in the stator teeth and yoke. The optimizer chooses the



(a) Torque profiles of the initial and optimized motor for $J \in J_0 \cdot \{0, 0.5, 1\}$. The markers highlight the evaluated angles in the optimization process.



(b) Percentage change of torque ripple plotted over the electric phase offset and the phase current. The torque ripple decreases significantly over a large range of operating points.

Fig. 4: Comparison of initial and optimized torque profiles for different operating points.

teeth and yoke width such that the saturation of the iron is optimally exploited.

- In contrast to the rotor surface, the stator surface remains almost unchanged and circular. This means that adapting the rotor surface has the most relevant influence to reduce the torque ripple.
- The thickness of the iron bridges in the rotor are reduced. This allows for a smaller magnet size but increases mechanical stresses at the bridges.
- The optimization sets the motor length to the minimum value and compensates this with increased radial scale. In order to find the best motor length, mechanical stress constraints need to be added in the future such that the radial scale is not increased arbitrarily.

A comparison of the torque profiles for the initial and optimized motor is found in Fig. 4. In Fig. 4a the initial and optimized torque profiles for the three operating points that were used for optimization are compared. Fig. 4b shows the percentage change of the torque ripple depending on J and φ_0 . It becomes clear that the torque ripple is drastically reduced. Especially near to the optimized $\varphi_0 = -11.6^\circ$ and for low J the torque ripple is decreased. Only outside the usual operating points \hat{T} can slightly increase.

IV. CONCLUSION

In this paper, we have optimized a PMSM for multiple operating points by adjusting both rotor and stator parameters and shape as well as the axial and radial dimensions by enhancing the framework from [6]. We have shown that several objectives (cost, torque ripple, losses) can be reduced simultaneously. Despite having a large number of optimization variables, the nonlinear optimization converges quickly due to the use of gradient based optimization involving analytical expressions. For future research, including demagnetization and mechanical stresses in the optimization process are key aspects to guarantee the feasibility of the generated designs.

ACKNOWLEDGMENT

The work of Michael Wiesheu and Theodor Komann is supported by the joint DFG/FWF Collaborative Research Centre CREATOR (CRC – TRR361/F90) at TU Darmstadt, TU Graz and JKU Linz as well as the Graduate School CE within the Centre for Computational Engineering at TU Darmstadt.

REFERENCES

- [1] Aissam Riad Meddour et al. “Optimization of the Lifetime and Cost of a PMSM in an Electric Vehicle Drive Train”. In: *Energies* 16.13 (2023). ISSN: 1996-1073. DOI: [10.3390/en16135200](https://doi.org/10.3390/en16135200). URL: <https://www.mdpi.com/1996-1073/16/13/5200>.
- [2] Sergio I. Suriano-Sánchez et al. “A Review of Torque Ripple Reduction Design Methods for Radial Flux PM Motors”. In: 3.4 (2022), pp. 646–661. DOI: [10.3390/eng3040044](https://doi.org/10.3390/eng3040044).
- [3] Mohd. Fairuz Bin Omar et al. “Design Optimization Methods for Electrical Machines: A Review”. In: *Journal of Electrical Engineering & Technology* 18.4 (2022), pp. 2783–2800. ISSN: 2093-7423. DOI: [10.1007/s42835-022-01358-y](https://doi.org/10.1007/s42835-022-01358-y).
- [4] Melina Merkel, Peter Gangl, and Sebastian Schöps. “Shape Optimization of Rotating Electric Machines using Isogeometric Analysis”. In: 36.4 (Feb. 2021). DOI: [10.1109/TEC.2021.3061271](https://doi.org/10.1109/TEC.2021.3061271). arXiv: [1908.06009](https://arxiv.org/abs/1908.06009).
- [5] FNU Nishanth and Bingnan Wang. “Topology Optimization of Electric Machines: A Review”. In: *2022 IEEE Energy Conversion Congress and Exposition (ECCE)*. 2022, pp. 1–8. DOI: [10.1109/ECCE50734.2022.9948073](https://doi.org/10.1109/ECCE50734.2022.9948073).
- [6] Michael Wiesheu et al. *Combined Parameter and Shape Optimization of Electric Machines with Isogeometric Analysis*. 2023. eprint: [2311.06046](https://arxiv.org/abs/2311.06046).
- [7] Michael Wiesheu. *MichaelWiesheu/ICEMsnapshot: 0.0.0*. Version placeholder. Feb. 2024. DOI: [10.5281/zenodo.10726571](https://doi.org/10.5281/zenodo.10726571).

- [8] Herbert Egger et al. “On torque computation in electric machine simulation by harmonic mortar methods”. In: 12.6 (2022). DOI: [10.1186/s13362-022-00121-2](https://doi.org/10.1186/s13362-022-00121-2). arXiv: [2112.05572](https://arxiv.org/abs/2112.05572).
- [9] Zeger Bontinck et al. “Isogeometric Analysis and Harmonic Stator-Rotor Coupling for Simulating Electric Machines”. In: 334 (2018), pp. 40–55. DOI: [10.1016/j.cma.2018.01.047](https://doi.org/10.1016/j.cma.2018.01.047). arXiv: [1709.05301](https://arxiv.org/abs/1709.05301).
- [10] Sheppard J. Salon. *Finite Element Analysis of Electrical Machines*. Kluwer, 1995.
- [11] Uwe Pahner. “A General Design Tool for the Numerical Optimisation of Electromagnetic Energy Transducers”. PhD Thesis. Leuven: KU Leuven, May 1998.
- [12] Martin Nell, Jonas Lenz, and Kay Hameyer. “Scaling laws for the FE solutions of induction machines”. In: *Archives of Electrical Engineering* 68 (Sept. 2019), pp. 677–695. DOI: [10.24425/ae.2019.129350](https://doi.org/10.24425/ae.2019.129350).
- [13] Stjepan Stipetic, Damir Žarko, and Mircea Popescu. “Scaling laws for synchronous permanent magnet machines”. In: *2015 Tenth International Conference on Ecological Vehicles and Renewable Energies (EVER)*. 2015, pp. 1–7. DOI: [10.1109/EVER.2015.7113006](https://doi.org/10.1109/EVER.2015.7113006).
- [14] Nicola Bianchi. *Electrical Machine Analysis Using Finite Elements*. Boca Raton: Taylor & Francis, 2005.
- [15] Rafael Vázquez. “A new design for the implementation of isogeometric analysis in Octave and Matlab: GeoPDEs 3.0”. In: 72.3 (Aug. 2016), pp. 523–554. DOI: [10.1016/j.camwa.2016.05.010](https://doi.org/10.1016/j.camwa.2016.05.010).
- [16] D. C. Meeker. *Finite Element Method Magnetics*. Version 4.2. 2018. URL: <https://www.femm.info>.